Optical Sensing of Electron-Beam Position With Twin Silver Nanotube Antenna Tuned to Hybrid Surface Plasmon Resonance

Dariia O. Herasymova, *Student Member, IEEE*, Sergii V. Dukhopelnykov, *Member, IEEE*, Mario Lucido, *Senior Member, IEEE*, and Alexander I. Nosich, *Fellow, IEEE*

***Abstract*—Considered is the diffraction radiation of a flat modulated beam of electrons flowing between two identical circular nanotubes made of silver. The electromagnetic field of such a beam is a two-dimensional H-polarized surface wave, which propagates in the same direction as the beam, with the phase velocity equal to the beam velocity. This field excites the currents on the nanotubes that radiate even if the beam does not touch the scatterers. For numerical solution, we use the method of partial separation of variables and the addition theorems for cylindrical functions that reduces the diffraction radiation problem to a matrix equation. On casting this equation to the Fredholm second-kind form, we compute far-field scattering cross-sections and field patterns with controlled accuracy. The obtained results show that a shift of the beam trajectory from the central-symmetric position triggers the excitation of certain resonances, which are absent otherwise. This may serve as a basis for the design of novel optical-range beam position monitors of nanoscale dimensions.**

***Index Terms*—Diffraction radiation, nanotube dimer, electron beam, plasmon resonance, beam position monitor.**

I. Introduction

DIFFRACTION Radiation (DR) is a broadly defined effect of the electromagnetic wave radiation caused by the electron beams passing near to material objects. Thus, DR can be observed in a wide range of frequencies. For instance, visible-light DR from the electron beam moving across a grating is also known as the Smith-Purcell effect [1]. It was discovered in the 1950s and then studied theoretically in [2]–[10] and other publications. The term DR was coined to distinguish such radiation of charged particles from the other radiation effects, e.g. the transition radiation (TR), emitted when the electromagnetic field, which accompanies a moving beam, polarizes atoms of the material object, the boundary of which it is crossing. In contrast, DR is the radiation of the polarization and surface currents induced by the electron beam on the scatterers located in the proximity to its trajectory, without crossing their boundaries.

The use of DR effect is a promising approach in the particle beam diagnostics, offering a noninvasive technique of remote sensing of the beam position and velocity in accelerators and colliders. It is already exploited in the microwave range beam-position monitors (BPM) [11]–[17]. Optical-range DR, i.e. infrared, visible-light and ultraviolet waves emitted by nanoscale scatterers, which are available today due to the progress of nanotechnology, opens new ways in the BPM design [18]–[21].

Small size of nanoscatterer suggests that its effect on the beam velocity and trajectory can be neglected, so that one can consider them as fixed values. In such case, the modeling of the DR effect can be performed using linear formulation, as a problem of classical electromagnetic-wave scattering theory. Here, the incident wave is a given field of the beam in the free space, that is scattered and absorbed by the scatterers of given size, shape, and material parameters.

Measuring the DR fields in the near or far zone, one can judge about the electron-beam parameters and control them. To improve the DR BPM performance, it is necessary to find optimal configuration of its elements and materials. A common approach is to use the resonance effects. This enhances the DR effect, at the resonance frequency, in direct proportion to the Q-factor of resonance. In the microwave range, various hollow cavities, which are usually coaxial with the drift tubes, are used in BPM design. This approach can be extended to the optical DR effect if suitable nanoscale resonances on the sub-wavelength scatterers are found. Such resonances can be obtained using high-refractive-index materials; however, the available today materials have refractive indices within several dozens, so that the nanoscale resonators have only moderately sub-wavelength dimensions [22]. As an alternative, truly nanoscale resonance effect is related to the localized surface plasmon (LSP) modes of deeply sub-wavelength noble-metal particles and wires. Here, two metals are especially attractive: the gold, because of its chemical stability, and the silver, due to the smallest optical losses.

However, the LSP modes of solid circular metal wires are H-polarized and appear in every azimuthal order, characterized with the index $m = 1, 2, \ldots$ For a wire of the radius a in the

Manuscript received April 1, 2020; revised July 16, 2020 and September 11, 2020; accepted September 11, 2020. Date of publication September 15, 2020; date of current version October 29, 2020. This work was supported by the National Research Foundation of Ukraine, under Project 2020.02.0150. *(Corresponding author: Dariia O. Herasymova.)*

Dariia O. Herasymova, Sergii V. Dukhopelnykov, and Alexander I. Nosich are with the Laboratory of Micro and Nano Optics, Institute of Radio-Physics and Electronics of the National Academy of Sciences of Ukraine, Kharkiv 61085, Ukraine (e-mail: dariia.heras@gmail.com; dukh.sergey@gmail.com; anosich@yahoo.com).

Mario Lucido is with the Department of Information and Electronic Engineering, University of Cassino and Southern Lazio, 03043 Cassino, Italy (e-mail: lucido@unicas.it).

Color versions of one or more of the figures in this article are available online at https://ieeexplore.ieee.org.

Digital Object Identifier 10.1109/JSTQE.2020.3024114

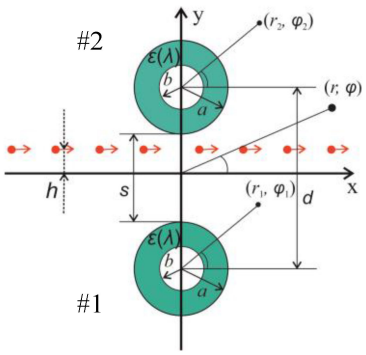

Fig. 1. Cross-sectional geometry of electron beam moving between two identical circular silver nanotubes.

free space, their wavelengths, λ_m, are clustered at the root of approximate m-independent quasi-static equation, $\mathrm{Re}\,\varepsilon(\lambda_m) = -1 + O(a^2/m\lambda^2)$,where $\varepsilon(\lambda)$ is dielectric function of metal [23]–[26]. Besides, Q-factors of all LSP modes are low, of the order of $O(\mathrm{Im}^{-1}\varepsilon)$. Together, these circumstances make the use of such wires pointless.

A search for possible metal nanoscatterers, which are more promising for BPM, yields two shapes, which support optical LSP modes that are spectrally distanced for different m. These are "flower" solid nanowires and hollow circular wires, i.e. nanotubes. In the first case, spectral shift of the m-th LSP is controlled by the angular periodicity [27], and in the second it strongly depends on the tube thickness [28], [29]. However, the LSP mode Q-factors of any solid nanowire remain low, while for a nanotube the inner and outer LSP modes of every azimuth index m hybridize and Q-factors of the "difference" family behave as $O[\mathrm{Im}^{-1}\varepsilon(a-b)^{-1}a]$. Hence, they can be rather high, and the manufacturing of such nanotubes is quite realistic [30]. This makes noble-metal nanotubes more attractive as resonance scatterers in optical applications.

In 2-D, however, the design of BPM sensor must include not a single but two identical elements, for instance, the edges of a slot [11]. Then a difference in the DR between the opposite sides of the beam trajectory can indicate a shift in beam position. Following this logic, twin dielectric and metal nanowire configurations were studied numerically in [31], [32], respectively. Note that plasmonic dimers are an object of active research in today's photonics [33], [34].

In the current work, we analyze another possible BPM configuration, based on the dimer of twin silver nanotubes as shown in Fig. 1. In the analysis, we follow that of [32], modified to account for the inner void in each tube. Our goal is to investigate how the position of the beam trajectory influences the power of DR and the appearance of resonances on the hybrid LSP "supermodes" of such dimer.

II. Problem Formulation and Basic Equations

We investigate an unbounded two-dimensional (2-D) beam of electrons passing along the straight trajectory at the distance h from the x-axis, with a fixed velocity $v = \beta c$, where c is the light velocity and $\beta < 1$. The charge density function, if modulated in time in harmonic manner, is

$$\rho = \rho_0 \delta(y-h)\exp[i(kx/\beta - \omega t)], \tag{1}$$

where $\delta(\cdot)$ is the Dirac delta function, ω and ρ_0 are the frequency and the amplitude of the beam modulation, and $k = \omega/c$ is the free-space wavenumber. Note that a harmonic modulation of the electron density can be achieved by the preliminary bunching of the beam in a periodic waveguide or directly, using external laser [17].

According to [2], [3], the field of the beam (1) in the free space is the H-polarized slow surface wave propagating along the x-axis, with the magnetic-field z-component

$$H_z^0(x,y) = A\,\beta \mathrm{sign}(y-h) e^{-q|y-h|} e^{i(k/\beta)x} \tag{2}$$

where $q = k\gamma/\beta$, $\gamma = (1-\beta^2)^{1/2}$ is inverse Lorentz factor, the function $\mathrm{sign}(\cdot) = \pm 1$ is the sign of the expression in the brackets, the time dependence is omitted, and A is a known constant. Note that the field (2) has finite jump at the trajectory, corresponding to the presence of the current, and decays exponentially in the normal direction. The rate of that decay is faster for the electron beams with $\beta \ll 1$.

Considered BPM configuration is shown in Fig. 1. Two circular silver nanotubes (#1 and #2) have the same outer radius a, inner radius b, and refractive index $\alpha(\lambda) = \sqrt{\varepsilon}$. They are separated by the air-gap s, with d being the distance between their axes. We assume that beam of particles (1) passes between the tubes in parallel to the x direction at the distance h from it surface. The Cartesian and the local and global polar coordinates are chosen as depicted in Fig. 1.

The formulation of the 2-D wave-scattering problem for the DR field, i.e. the scattered field function, involves the Helmholtz equation, the penetrable-boundary conditions at tube contours, the Sommerfeld radiation condition at infinity, and the condition of local power finiteness. The solution uniqueness is guaranteed by these conditions.

Inside each void and tube (domains I and II), we expand the field in the azimuthal Fourier series, respectively,

$$H_z^{\mathrm{int}(p),I}(r,\varphi) = \sum_{m=-\infty}^{\infty} y_m^{(p)} J_m(kr_p) e^{im\varphi_p},\ r_p < b, \tag{3}$$

$$H_z^{\mathrm{int}(p),II}(r,\varphi) = \sum_{m=-\infty}^{\infty} \left[c_m^{(p)} J_m(k\alpha r_p) + d_m^{(p)} H_m(k\alpha r_p)\right] e^{im\varphi_p},$$

$$b < r_p < a,\quad p = 1,2 \tag{4}$$

and seek the scattered field (DR field) as follows:

$$H^{sc}(r,\varphi) = \sum_{p=1,2} \sum_{m=-\infty}^{+\infty} z_m^{(p)} H_m(kr_p)\, e^{im\varphi_p},\quad r_p > a, \tag{5}$$

In (3) to (5), $H_m(\cdot)$ and $J_m(\cdot)$ are the Hankel (first-kind) and the Bessel functions, respectively. At the inner wall of each tube, at $r_p = b,\ \ p = 1,2$, the boundary conditions demand that both H_z and E_{φ_p} are continuous,

$$H_z^{\mathrm{int}(p),I} = H_z^{\mathrm{sin}\,t(p),II},\quad E_{\varphi_p}^{\mathrm{int}(p),I} = E_{\varphi_p}^{\mathrm{int}(p),II} \tag{6}$$

As these conditions are valid for all $0 \le \varphi_p < 2\pi$, they allow us to exclude some of the unknown coefficients. The boundary conditions at $r_p = a$ and $0 \le \varphi_p < 2\pi$ are

$$H_z^{\text{int}(p),II} = H_z^0 + H_z^{sc}, \quad E_{\varphi_p}^{\text{int}(p),II} = E_{\varphi_p}^0 + E_{\varphi_p}^{sc} \tag{7}$$

Substituting into (7) the series expressions (4), (5) and a similar expansion of the beam field (2) [31], and introducing new unknowns, $\tilde{z}_n^{(p)} = z_n^{(p)} w_n,\ w_n = |n|!(2/ka)^{2|n|}$, we derive two coupled infinite-matrix equations ($p \ne j = 1, 2$),

$$\tilde{z}_m^{(p)} + \sum_{n=-\infty}^{+\infty} (\mp i)^{n-m} J_n(ka) H_{m-n}(kd) V_m P_m^{-1} \tilde{z}_n^{(j)} = \left[f_m^{(p)} F'_m - f_m'^{(p)} F_m \right] P_m^{-1}, \quad m = 0, \pm 1, \pm 2, \ldots, \tag{8}$$

where the prime denotes the differentiation in argument and

$$V_m = J_m(ka) F'_m - J'_m(ka) F_m, \tag{9}$$

$$P_m = w_m^{-1} \left[H_m(ka) F'_m - H'_m(ka) F_m \right], \tag{10}$$

$$F_m = J_m(k\alpha a) + H_m(k\alpha a) S_m(kb, \alpha), \tag{11}$$

$$F'_m = \alpha J'_m(k\alpha a) + \alpha H'_m(k\alpha a) S_m(kb, \alpha), \tag{12}$$

$$S_m(kb, \alpha) = \frac{\alpha J'_m(kb) J_m(k\alpha b) - J_m(kb) J_m'(k\alpha b)}{J_m(kb) H_m'(k\alpha b) - \alpha J'_m(kb) H_m(k\alpha b)}, \tag{13}$$

$$f_m^{(1,2)} = \mp A e^{-q(d/2 \pm h)} i^m J_m(ka) (1 \mp \gamma)^m \beta^{-m+1}, \tag{14}$$

Note that (8) reduces to the twin solid wire case equation (10) of [32] if $b \to 0$ that entails $S_m = y_m^{(p)} = d_m^{(p)} = 0$.

Similar to the twin solid-wire case of [32], the set (8) is the Fredholm second kind matrix equation of block type (see also [35]–[37]). Then the Fredholm theorems guarantee that its numerical solution (after truncation of each block to finite order N) converges to the exact solution for $N \to \infty$.

On using the large-argument asymptotic expressions for the Hankel functions, far from the scatterer ($r \to \infty$) the DR field takes the form of outgoing cylindrical wave,

$$H^{sc}(r, \varphi) = (2/i\pi kr)^{1/2} \exp(ikr) \Phi(\varphi), \tag{15}$$

where the angular pattern is a function of the global polar coordinate, φ. On the truncation of the matrix equation (8), this function depends on the coefficients $\tilde{z}_m^{(1,2)}$ as follows:

$$\Phi(\varphi, N) = \Phi_1(\varphi, N) + \Phi_2(\varphi, N),$$

$$\Phi_{1,2}(\varphi, N) = e^{\mp \frac{1}{2} ikd \sin\varphi} \sum_{m=-N}^{N} (-i)^m w_m^{-1} \tilde{z}_m^{(1,2)} e^{im\varphi} \tag{16}$$

Then, the partial scattering cross-sections (SCS), associated with the DR power radiated into the lower and the upper half-spaces [32], are found as

$$\sigma_{sc}^{(1,2)}(N) = 2\left(\pi k A^2\right)^{-1} \int_0^{\mp\pi} |\Phi(\varphi, N)|^2 d\varphi, \tag{17}$$

The partial absorption cross-sections (ACS) can be found from the Optical Theorem, adapted to the DR analysis [32],

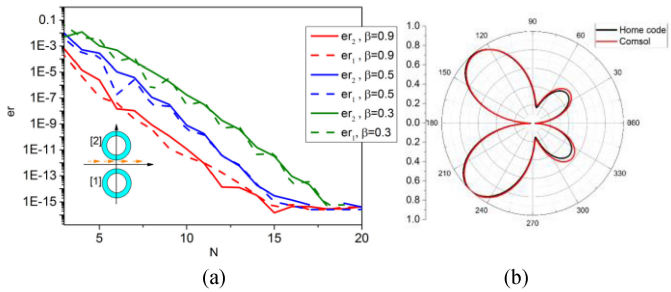

Fig. 2. Far-field computation error versus the matrix block truncation number N, for several beam velocities (a) and comparison of the far field patterns calculated by COMSOL and in-house code. BPM model consists of two silver tubes with radii $a = 50$ nm and $b = 45$ nm, separated by the air gap of $s = 20$ nm; beam shift is $h = 5$ nm and wavelength is $\lambda = 332$ nm.

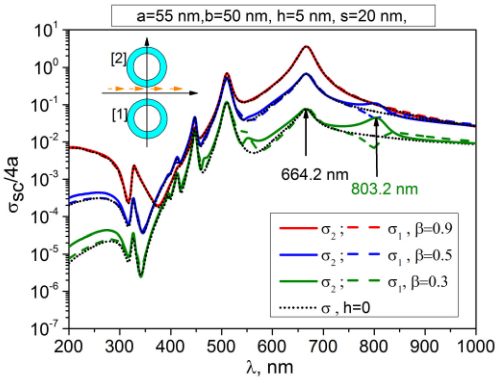

Fig. 3. Normalized partial SCS versus the wavelength for twin silver tubes with radii $a = 55$ nm, $b = 50$ nm, beam shift $h = 0$ and 5 nm, and air gap width $s = 20$ nm.

or, equivalently, through the integration of the Poynting vector flux over the outer contour of each nanotube,

$$\sigma_{abs}^{(1,2)}(N) = A^{-2} 2\pi a |\alpha|^{-2} \sum_{m=-N}^{N} |g_m^{(1,2)}|^2 \text{Im}\left(\alpha F_m F_m'^*\right), \tag{18}$$

where $F_m(\cdot)$and $F'_m(\cdot)$ are defined in (11) and (12), and

$$g_m^{(1,2)} = \frac{\pi}{2} kb\alpha y_m^{(1,2)} [\alpha J_m(kb) H'_m(k\alpha b) - J'_m(kb) H_m(k\alpha b)] \tag{19}$$

III. Numerical Results and Discussion

A. Convergence and Accuracy

In computations, we use experimental data of [38] for the dielectric function of silver. To check the code convergence for a varying matrix-block truncation order N and visualize its rate, we have computed the relative error, in the far-field SCS, with respect to the data computed at $N_{\max} = 30$,

$$er_{1,2}(N) = \left| \sigma_{sc}^{(1,2)}(N) - \sigma_{sc}^{(1,2)}(N_{\max}) \right| / \left| \sigma_{sc}^{(1,2)}(N_{\max}) \right| \tag{20}$$

The typical plots of such errors are presented in Fig. 2(a) . As visible, 5-6 digit accuracy in the far field is achieved if the

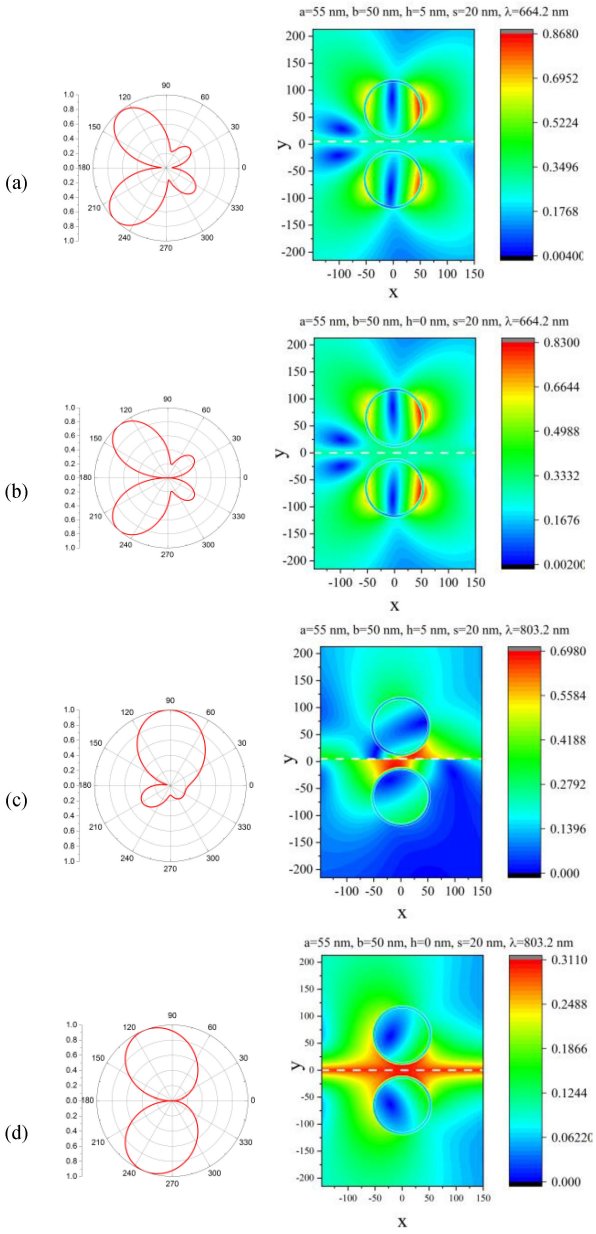

Fig. 4. In-resonance near magnetic field and far field scattering patterns of twin nanotube BPM with tube radii $a = 55$ nm, $b = 50$ nm, air gap width $s = 20$ nm and beam shift $h = 5$ nm (a), (c) and $h = 0$ (b), (d). The wavelengths are 664.2 nm for (a), (b) and 803.2 nm (c), (d), marked with arrows in Fig. 3.

truncation order is $N \geq \max[kd, (k\alpha a/\beta)]+5$. Thus, the slower the beam, the larger the matrix size N needed for the same accuracy. This is a result of the slower decay of the elements of the right-hand part vector (14) at $|m|\to\infty$, controlled by the factor $\beta^{-|m|}$. Equivalently, as $\beta < 1$, it means that electric size of the scatterer illuminated with the incident field (2) must be increased by the "beam factor," $1/\beta$, in comparison to the plane-wave scattering.

The far-field error is by an order smaller than the near-field error that is explained by the presence of the factor $1/w_m$ in (16). Note that the effect of β is the same both in the far and near zone: slower beams request larger matrices to be inverted, for

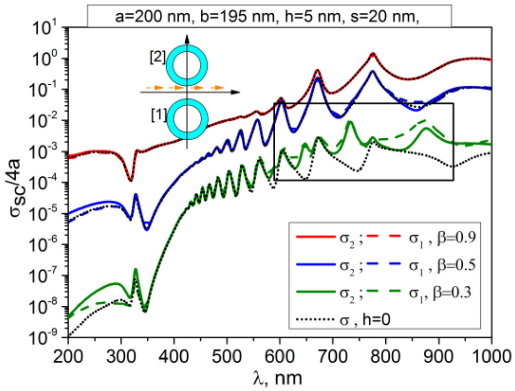

Fig. 5. The same as in Fig. 3 for twin silver tubes with radii $a = 200$ nm and $b = 195$ nm.

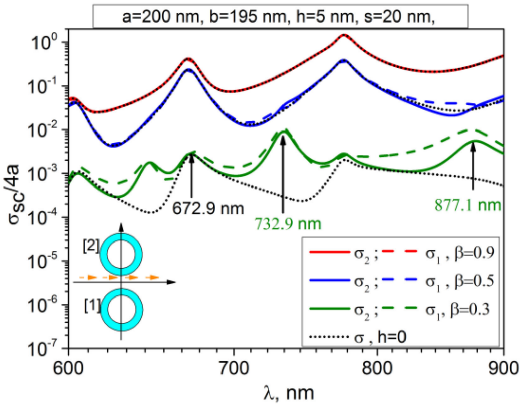

Fig. 6. Zoom of Fig. 5 between the wavelengths of 600 nm and 900 nm.

the same accuracy. Besides of β, the electric size of the whole dimer is to be accounted for when selecting N. Still besides, the rate of convergence degrades for very small values of the air gap width, s.

It should be noted that the tubes must not touch each other or the beam trajectory as in the either case the matrix equation (8) loses its Fredholm nature.

To support our results, we present, in Fig. 2(b), a comparison of two normalized far-field patterns, computed with our code based on (8) where $N = 30$ and with COMSOL commercial software. The agreement is quite good, while the computation time needed by COMSOL is approximately 30 times larger. Still, from the mathematical point of view, this comparison serves as a validation of COMSOL rather than our code because COMSOL's accuracy is not controlled.

B. Diffraction Radiation From Small-Radius Nanotubes

Keeping in mind BPM applications, we look for the features of DR that can serve as indicators of the beam shift from the central-symmetric position between the twin silver nanotubes. Therefore, we compute the spectra, in the visible-light range, of the partial SCS of the studied configuration, excited by symmetric and shifted beams. The plots in Fig. 3 correspond to the nanotubes of the 55-nm outer radius and 5-nm wall thickness,

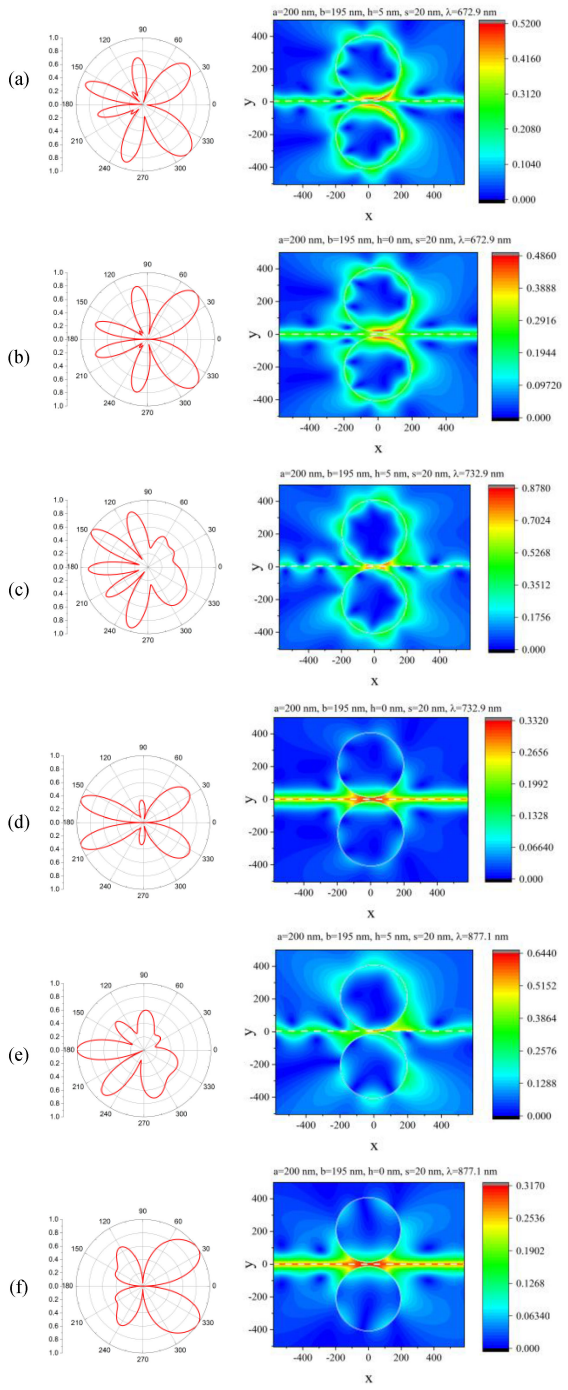

Fig. 7. In-resonance near magnetic field and far field scattering patterns of twin nanotube BPM with tube radii $a = 200$ nm, $b = 195$ nm, air gap $s = 20$ nm and beam shift $h = 5$ nm (c), (b) and $h = 0$ (b), (d). The wavelengths are 672.9 nm for (a), (b), 732.9 nm (c), (d), and 877.1 nm (e), (f), marked with arrows in Fig. 6.

with the air gap width $s = 20$ nm. Two trajectories of particles are considered: shifted by $h = 5$ nm (solid and dashed curves) and not shifted ($h = 0$, dotted curves), and three beam velocities, $\beta = 0.9,\ 0.5$, and 0.3. In each case, we can see sharp resonances on the hybrid LSP modes of silver tubes [28], [29].

More accurately, in a twin-circular-nanotube photonic plasmonic molecule, these modes hybridize further and form

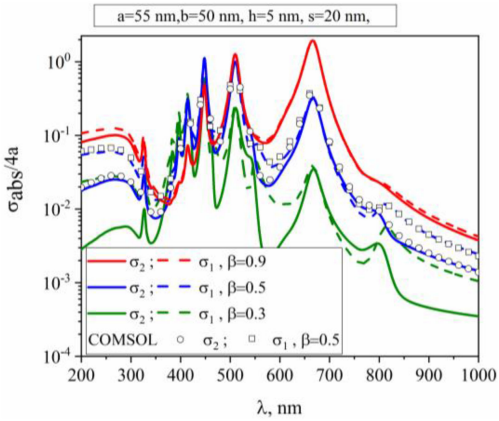

Fig. 8. Normalized partial ACS versus the wavelength for twin silver tubes with radii $a = 55$ nm, $b = 50$ nm, beam shift $h = 0$ and 5 nm, and air gap width $s = 20$ nm.

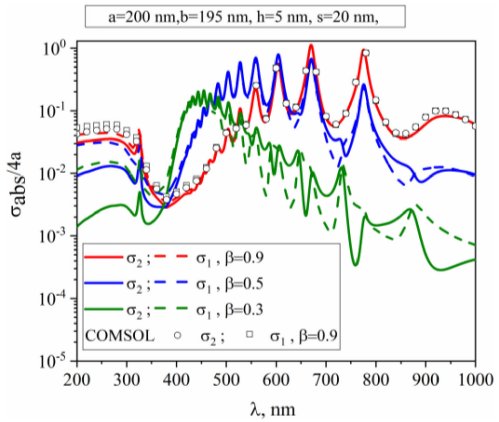

Fig. 9. The same as in Fig. 5 for twin silver tubes with radii $a = 200$ nm.

quartets of closely spaced "supermodes," with mode fields belonging to four classes of symmetry with respect to the x and y-axes [31], [32], [35].

The beam field (2) is anti-symmetric with respect to the beam trajectory.

Therefore, two of four "supermodes" of each type cannot be excited by the symmetrically flowing beam (they remain "dark") however they can shine if the beam is shifted ($h \neq 0$). Indeed, this is actually what we observe at $\lambda = 803$ nm in Fig. 3, provided that the beam is non-relativistic, $\beta = 0.3$.

Such interpretation is fully supported by the near-field patterns in the resonances, shown in Fig. 4. Panels (a) and (b) and (c) demonstrate the field portraits where the "dipole" LSP mode $P_1^{(-)}$ dominates on each tube; however, the field symmetry on (a), (b) is orthogonal to that on (c).

C. *Diffraction Radiation From Large-Radius Nanotubes*

The plots in Fig. 5 and Fig. 6 show the visible-light spectra of partial SCS for the pair of nanotubes with much larger radii of $a = 200$ nm and $b = 195$ nm, so that the wall thickness is again 5 nm, with the air-gap of $s = 20$ nm. The electron-beam velocities are the same as in the previous case. The trajectory shift is $h =$

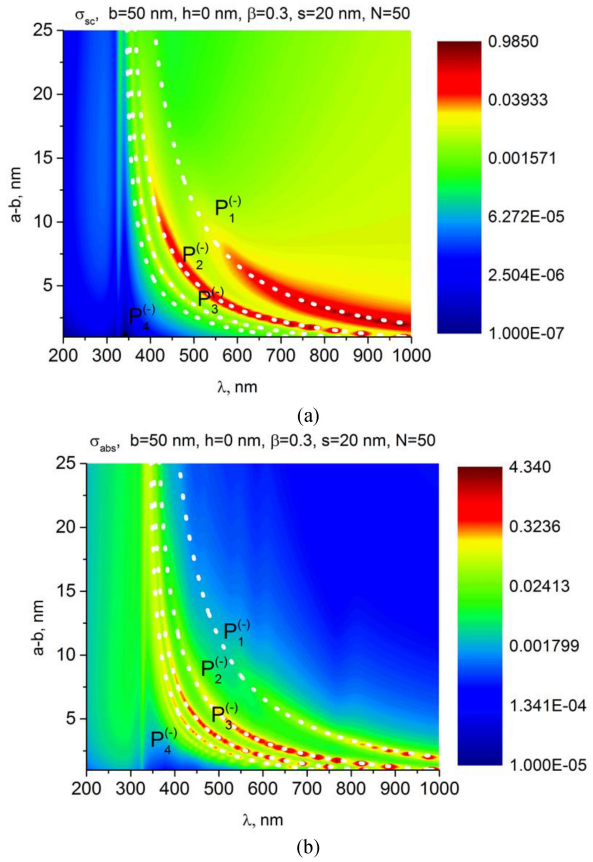

Fig. 10. Color maps of total SCS (a) and ACS (b) versus the wavelength and the tube thickness for twin silver tubes with inner radius $b = 50$ nm, air gap width $s = 20$ nm, beam velocity $\beta = 0.3$, and no beam shift ($h = 0$).

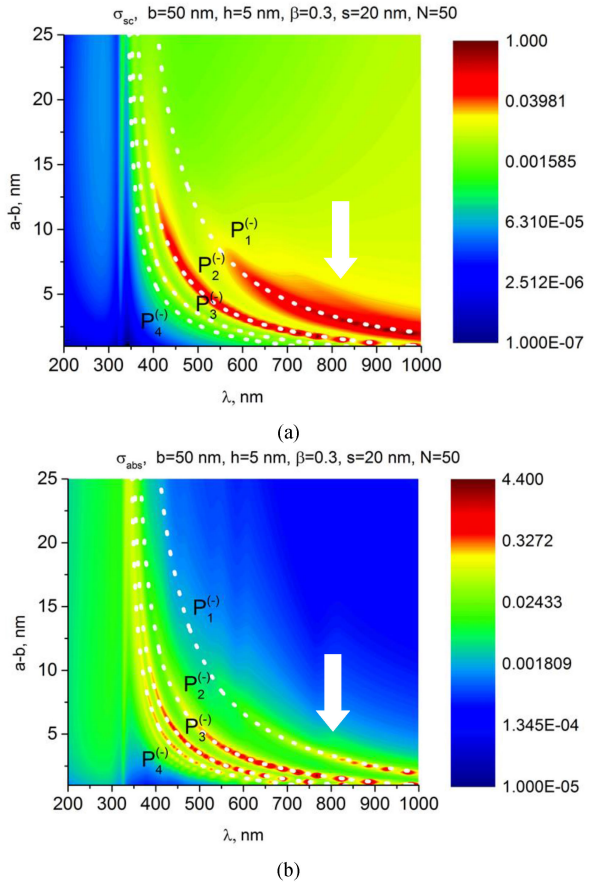

Fig. 11. The same as in Fig. 10 however for the beam shift $h = 5$ nm.

5 nm and the data for zero shift are also shown as dotted curves. As before, one can see the sharp resonance peaks of the DR power on the wavelengths of the hybrid LSP supermodes of the silver tubes. They form a nearly periodic sequence where each peak corresponds to different azimuth index, $m = 1,2, \ldots$. Note that they are much sharper than the collective LSP peaks in the DR power for electron-beam excited solid silver nanowire or a pair of them [22], [32].

Similarly to the previous case, some of the peaks appear only if the beam is shifted from the center of the air-gap. For instance, this takes place at $\lambda = 733$ nm and 877 nm.

The corresponding to them hybrid LSP supermodes of twin nanotubes remain "dark" under the excitation by the centrally flowing beam, the field (2) of which is orthogonal to their eigenfields in symmetry. These modes, however, start resonating (i.e. become "bright") if the beam is shifted, because this leads to appearance of the part of the incident field that matches the mode symmetry.

The in-resonance near-field patterns in Fig. 7 correspond to the frequencies marked with arrows in Fig. 6. They reveal that the higher-order LSP modes $P_3^{(-)}$ dominate on each tube on panels (a), (b) and (c), however, with different "supermode" symmetries. On panel (e), the field of LSP mode $P_2^{(-)}$ can be identified. The peaks at the shorter wavelengths correspond to the larger LSP indices m.

D. Absorption of Light by Twin Nanotubes

As the silver is sizably lossy in the visible-light range, the absorbed in the nanotubes power is not expected to be small. We characterize this power with the aid of two partial ACS, given by (18). In Fig. 8 and Fig. 9, we present the spectra of ACS for the same two configurations of twin-nanotube BPM as in Sub-sections III-B and III-C, respectively, however only for the case of the trajectory, shifted by 5 nm from the central-symmetrical position. They show the resonances on the hybrid LSP supermodes of twin silver nanotubes. As discussed above, some of these supermodes are not excited by a non-shifted beam. In general, one can see that the absorption in nanotubes is roughly by an order of magnitude larger than the scattering. This is in full agreement with similar relationship between the plane-wave scattering and absorption by metal nanoparticles in the visible range [23], [24].

To provide a better vision of the dependence of total SCS and ACS on the wavelength and the tube wall thickness, we present the color maps of these quantities for the not-shifted and shifted beam in Fig. 10 and Fig. 11, respectively. White dashed curves are predicted by the quasi-static analysis of hybrid LSP modes $P_m^{(-)}$ of stand-alone nanotube, see [28]. These maps visualize the resonance on the supermode $P_1^{(-)}$ of the y-even family, marked with arrow, which is present if $h = 5$ nm, however remains "dark" if the beam is not shifted.

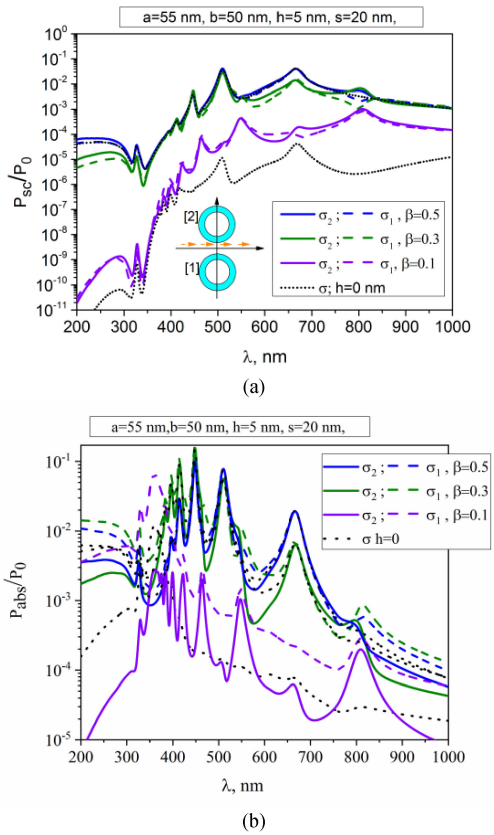

Fig. 12. Partial SCS (a) and ACS (b) versus the wavelength for twin silver tubes with radii $a = 55$ nm, $b = 50$ nm, beam shift $h = 5$, velocity β, and air gap width $s = 20$ nm.

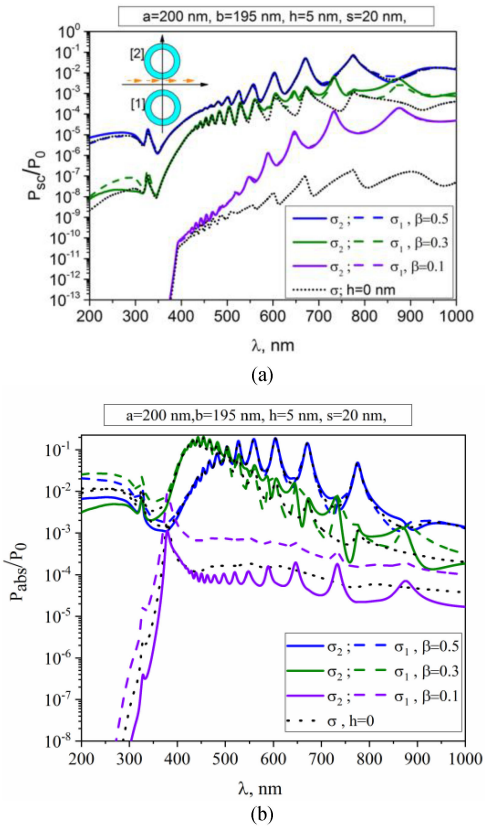

Fig. 13. The same as in Fig. 12 however for twin silver tubes with radii $a = 200$ nm, $b = 195$ nm.

E. Estimation of Electron-Beam Power Loss

Presented above are the data for partial and total SCS and ACS, which are traditional quantities in the analysis of optical scattering. Together, they yield the extinction cross-section, which characterizes the total power taken from the incident field in the presence of scatterers. Still, unlike the traditional plane-wave scattering, the power carried by the beam field (2) through the plane, normal to its trajectory, is finite. This power is given by the equation

$$P_0 = A^2 Z_0 \beta^2 (k\gamma)^{-1} \tag{21}$$

Therefore, it is useful to compare (21) with the scattered and the absorbed powers, given by $P_{sc/abs} = {}^1\!/_2 \beta \sigma_{sc/abs}$. In Fig. 12 and 13, we show the spectra of the normalized quantities, P_{sc}/P_0 and P_{abs}/P_0, computed via the data of Fig. 3 and 5, respectively. As one can see, if the beam velocity does not exceed $\beta = 0.5$, the radiated power remains below 5% of the beam power even in the resonances, both for small ($a = 55$ nm) and large ($a = 200$ nm) nanotube dimers.

The power, absorbed in the silver nanotubes, is several dozen times larger than the DR power, and in the LSP-mode resonances it can exceed 50% if $\beta = 0.5$ for a small-tube dimer and even 70% for a large-tube dimer.

This result shows that, firstly, the absorption plays more important part than the scattering, in the total reduction of the beam power. This reminds us that even the most sophisticated particle accelerators sometimes suffer of unwanted heating incidents [39]. Secondly, it tells that the fundamental assumption of the DR modeling, that the beam is not influenced by the presence of imperfect scatterers, holds true only provided that the scatterers are not tuned to high-Q resonances and, generally speaking, if the beam is not relativistic. For the twin nanotubes studied here, the safe limit, in terms of velocity, is around $\beta = 0.2$: then the total power loss of the beam is within 10%, some 1% of which goes to DR and the rest – to the heating. To widen the area of applicability of the DR model, one should consider the configurations, where the scatterers are placed at the larger distances from the beam trajectory.

IV. Conclusion

We have shown, using a trusted and efficient in-house computational instrument, that the modulated beam of charged particles can be monitored noninvasively by measuring the power of the diffraction radiation, which occurs when the beam passes between two identical silver nanotubes. This power, as a function of the modulation wavelength, displays sharp peaks on the hybrid LSP supermodes of twin nanotubes. Some of these modes are excited only if the beam trajectory is shifted away from the central-symmetrical position, due to the symmetry properties of the corresponding supermode field. This effect can be used in the design of optical-range beam position monitors. We have also shown, for the first time in our opinion, that the area of good adequacy of the DR model is limited, in the presence of

nanoscale nanospaced resonant scatterers, to the non-relativistic beam velocities.

REFERENCES

[1] S. J. Smith and E. M. Purcell, "Visible light from localized surface charges moving across a grating," *Phys. Rev.*, vol. 92, 1953, Art. no. 1069.

[2] V. G. Sologub *et al.*, "Excitation of an electromagnetic field by an electron beam traveling close to a diffraction grating," *Radiophys. Quant. Electron.*, vol. 11, no. 4, pp. 327–333, 1968.

[3] P. M. van den Berg, "Smith-Purcell radiation from a line charge moving parallel to a reflection grating," *J. Opt. Soc. Am.*, vol. 63, no. 6, pp. 689–698, 1973.

[4] A. P. Potylitsyn, "Resonant diffraction radiation and Smith-Purcell effect," *Phys. Lett. A*, vol. 238, pp. 112–116, 1998.

[5] A. I. Nosich, "Diffraction radiation which accompanies the motion of charged particles near an open resonator," *Radiophys. Quant. Electron.*, vol. 24, no. 8, pp. 696–701, 1981.

[6] L. A. Pazynin and V. G. Sologub, "Radiation of a point charge moving uniformly along the axis of a narrow cylindrical ring," *Radiophys. Quant. Electron.*, vol. 25, no. 1, pp. 64–68, 1982.

[7] L. A. Pazynin and V. G. Sologub, "Diffraction radiation of a point charge moving along the axis of a segment of a circular waveguide," *Radiophys. Quant. Electron.* vol. 27, no. 10, pp. 816–822, 1984.

[8] L. A. Pazynin *et al.*, "Excitation of a cylindrical retarding system of finite length by a modulated flux of charge particles," *Radiophys. Quant. Electron.*, vol. 30, no. 4, pp. 376–387, 1987.

[9] A. I. Boltonosov and V. G. Sologub, "Excitation of an open strip-type resonator by a modulated beam of charged particles," *Sov. J. Communic. Technol. Electron.*, vol. 33, no. 6, pp. 133–140, 1988.

[10] G. I. Zaginaylov *et al.*, "Modeling of plasma effect on the diffraction radiation of relativistic beam moving over a grating of finite extent," *Microwave Opt. Technol. Lett.*, vol. 16, no. 1, pp. 50–54, 1997.

[11] M. Castellano, "A new non-intercepting beam size diagnostics using diffraction radiation from a slit," *Nucl. Instrum. Meth. A*, vol. 394, pp. 275–280, 1997.

[12] A. P. Potylitsyn, "Resonant diffraction radiation and Smith-Purcell effect," *Phys. Lett. A*, vol. 238, pp. 112–116, 1998.

[13] M. Castellano *et al.*, "Measurements of coherent diffraction radiation and its application for bunch length diagnostics in particle accelerators," *Phys. Rev. E*, vol. 63, 2001, Art. no. 056501.

[14] C. Boccard *et al.*, "Embedded collimator beam position monitors," in *Proc. Eur. Workshop Beam Diagnostics Instrum. Part. Accel.*, 2011, pp. 80–82.

[15] G. Valentino *et al.*, "Successive approximation algorithm for beam-position-monitor-based LHC collimator alignment," *Phys. Rev. Spec. Top. Accel. Beams*, vol. 17, no. 2, 2014, Art. no. 021005.

[16] Y. A. Goponov, R. A. Shatokhin, and K. Sumitani, "Diffracted diffraction radiation and its application to beam diagnostics," *Nucl. Instrum. Meth. A*, vol. 885, pp. 134–138, 2018.

[17] L. Bobb *et al.*, "Feasibility of diffraction radiation for noninvasive beam diagnostics as characterized in a storage ring," *Phys. Rev. Accel. Beams*, vol. 21, 2018, Art. no. 03801.

[18] T. Muto *et al.*, "Observation of incoherent diffraction radiation from a single-edge target in the visible-light region," *Phys. Rev. Lett.*, vol. 90, no. 10, pp. 104801–104804, 2003.

[19] P. Karataev *et al.*, "Beam-size measurement with optical diffraction radiation at KEK accelerator test facility," *Phys. Rev. Lett.*, vol. 93, 2004, Art. no. 244802.

[20] M. Bergamaschi *et al.*, "Noninvasive micrometer-scale particle-beam size measurement using optical diffraction radiation in the ultraviolet wavelength range," *Phys. Rev. Appl.*, vol. 13, no. 1, 2020, Art. no. 014041.

[21] N. Talebi, "Interaction of electron beams with optical nanostructures and metamaterials: From coherent photon sources towards shaping the wave function," *J. Opt.*, vol. 19, 2017, Art. no. 103001.

[22] D. O. Yevtushenko *et al.*, "Modeling of optical diffraction radiation from a dielectric and a silver nanowire excited by a modulated electron beam," *Opt. Quant. Electron.*, vol. 51, no. 1, 2019, Art. no 29.

[23] C. F. Bohren and D. R. Huffman, *Absorption and Scattering of Light by Small Particles*. Hoboken, NJ, USA: Wiley, 2004.

[24] L. Novotny and B. Hecht, *Principles of Nano-Optics*. Cambridge, U.K.: Cambridge Univ. Press, 2012.

[25] B. S. Lukyanchuk and V. Ternovsky, "Light scattering by a thin wire with a surface-plasmon resonance: Bifurcations of the Poynting vector field," *Phys. Rev. B*, vol. 73, 2006, Art. no. 235432.

[26] J. P. Kottmann and O. J. F. Martin, "Plasmon resonant coupling in metallic nanowires," *Opt. Express*, vol. 8, no. 12, pp. 655–663, 2001.

[27] E. V. Podivilov, B. I. Sturman, and M. V. Gorkunov, "Plasmonic resonances of nanowires with periodically corrugated cross sections," *J. Opt. Soc. Am. B*, vol. 29, no. 12, pp. 3248–3252, 2012.

[28] E. A. Velichko and A. I. Nosich, "Refractive-index sensitivities of hybrid surface-plasmon resonances for a core-shell circular silver nanotube sensor," *Opt. Lett.*, vol. 38, no. 23, pp. 4978–4981, 2013.

[29] E. A. Velichko *et al.*, "Localized versus delocalized surface plasmons: Dual nature of resonances on a silver circular wire and a silver tube of large diameter," *J. Opt.*, vol. 20, no. 7, 2018, Art. no. 075002.

[30] A. Murphy *et al.*, "Fabrication and optical properties of large-scale arrays of gold nanocavities based on rod-in-a-tube coaxials," *Appl. Phys. Lett.*, vol. 102, 2013, Art. no. 103103.

[31] D. O. Yevtushenko *et al.*, "Electron beam excitation of supermodes of a photonic molecule built on twin high refractive index dielectric nanowires," *J. Appl. Phys.*, vol. 125, no. 22, 2019, Art. no. 223102.

[32] D. O. Yevtushenko *et al.*, "Visible light from modulated electron beam moving between twin circular silver nanowires forming plasmonic molecule," *J. Opt.*, vol. 22, no. 2, 2020, Art. no. 025002.

[33] B. Gerislioglu *et al.*, "Monolithic metal dimer-on-film structure: New plasmonic properties introduced by the underlying metal," *Nano Lett.*, vol. 20, pp. 2087–2093, 2020.

[34] B. Gerislioglu *et al.*, "The role of $Ge_2Sb_2Te_5$ in enhancing the performance of functional plasmonic devices," *Materials Today Phys.*, vol. 12, 2020, Art. no. 100178.

[35] E. I. Smotrova, A. I. Nosich, T. M. Benson, and P. Sewell, "Optical coupling of whispering-gallery modes in two identical microdisks and its effect on photonic molecule lasing," *IEEE J. Sel. Top. Quant. Electron.*, vol. 12, no. 1, pp. 78–85, Jan.–Feb. 2006.

[36] D. M. Natarov *et al.*, "Effect of periodicity in the resonant scattering of light by finite sparse configurations of many silver nanowires," *Plasmonics*, vol. 9, no. 2, pp. 389–407, 2014.

[37] V. O. Byelobrov, T. L. Zinenko, K. Kobayashi, and A. I. Nosich, "Periodicity matters: Grating or lattice resonances in the scattering by sparse arrays of sub-wavelength strips and wires," *IEEE Antennas Propagat. Mag.*, vol. 57, no. 6, pp. 34–45, Dec. 2015.

[38] P. B. Johnson and R. W. Christy, "Optical constants of the noble metals," *Phys. Rev. B*, vol. 6, pp. 4370–4379, 1972.

[39] B. Salvant *et al.*, "Beam induced RF heating in LHC in 2015," in *Proc. Int. Part. Accel. Conf.*, 2016, pp. 602–605.

Dariia O. Herasymova (Student Member, IEEE) was born in Kharkiv, Ukraine, in 1993. She received the B.S. and M.S. degrees with honors in photonics and optical informatics from the Kharkiv National University of Radio Electronics, in 2017 and 2019, respectively. Since November 2019, she has been working towards the Ph.D. degree with the Institute of Radio-Physics and Electronics, National Academy of Sciences of Ukraine (IRE NASU), Kharkiv.

Since 2018, she has been with the Laboratory of Micro and Nano Optics, IRE NASU as a Junior Scientist. Her research interests include wave scattering and absorption, plasmon resonances, optical antennas, and eigenvalue problems. She was the recipient of the Pre-Doctoral Research Award of the IEEE Antennas and Propagation Society and Pre-Graduate Scholarship of the IEEE Microwave Theory and Techniques Society (2018) and the Young Scientist Prizes of the International Conferences on Mathematical Methods in Electromagnetic Theory (Kyiv, 2018) and on Direct and Inverse Problems of Electrodynamics (Tbilisi, 2018).

Sergii V. Dukhopelnykov, photograph and biography not available at the time of publication.

Mario Lucido, photograph and biography not available at the time of publication.

Alexander I. Nosich, photograph and biography not available at the time of publication.